THE AMERICAN SOCIETY OF MECHANICAL ENGINEERS
345 E. 47 St., New York, N.Y. 10017

87-GT-227

Measurements of the Unsteady Flow Field Within the Stator Row of a Transonic Axial-Flow Fan II — Results and Discussion

M.D. HATHAWAY
Propulsion Directorate
U.S. Army Aviation Research and Technology Activity — AVSCOM
Lewis Research Center,
Cleveland, Ohio 44135

K.L.SUDER
National Aeronautics and Space Administration
Lewis Research Center
Cleveland, Ohio 44135

T.H. OKIISHI
Iowa State University
Ames, Iowa 50010

A.J. STRAZISAR and J.J.ADAMCZYK
National Aeronautics and Space Administration
Lewis Research Center
Cleveland, Ohio 44135

ABSTRACT

Results of detailed unsteady velocity field measurements made within the stator row of a transonic axial-flow fan are presented. Measurements were obtained at midspan for two different stator blade rows using a laser anemometer. The first stator row consists of double-circular-arc airfoils with a solidity of 1.68. The second stator row features controlled-diffusion airfoils with a solidity of 0.85. Both stator configurations were tested at design-speed peak efficiency conditions. In addition, the controlled-diffusion stator was also tested at near-stall design-speed conditions. The procedures developed in Part I of this paper are used to identify the "rotor-wake-generated" and "unresolved" unsteadiness from the velocity measurements. (The term "rotor-wake-generated" unsteadiness refers to the unsteadiness generated by the rotor wake velocity deficit and the term "unresolved" unsteadiness refers to all of the remaining unsteadiness which contributes to the spread in the distribution of velocities such as vortex shedding, turbulence, etc.) Auto and cross correlations of these unsteady velocity fluctuations are presented in order to indicate their relative magnitude and spatial distributions. Amplification and attenuation of both rotor-wake-generated and unresolved unsteadiness are shown to occur within the stator blade passage.

NOMENCLATURE

N_S number of stator blades

R radius, cm

S distance measured along stator exit mean camber line, cm

V velocity magnitude, m/s

V_A average of stator inlet and exit velocities, m/s

V_{FS} freestream velocity, m/s

V_T total absolute velocity = $\sqrt{V_Z^2 + V_\theta^2}$, m/s

Γ stator blade circulation, m^2/s

Subscripts

I stator row inlet condition

E stator row exit condition

z axial component

r tangential component

1 measured component in direction of first beam orientation angle

2 measured component in direction of second beam orientation angle

Superscripts

$'$ fluctuating component

$\sim\sim$ ensemble average

$\overline{\quad}$ steady-state condition, or time average

AX axisymmetric component

INTRODUCTION

In the past, unsteadiness in turbomachines has been generally categorized as being either "periodic" or "random" ("turbulent"). Flow-field fluctuations resulting from the relative motion between blade rows have been categorized as "periodic" unsteadiness. "Random" unsteadiness has been used as a catch-all term which includes flow-field fluctuations due to turbulence, vortex shedding, global flow-field fluctuations, true random unsteadiness, and any other unsteadiness not correlated with rotor speed. Therefore, in the absence of a more descriptive terminology for unsteady

Presented at the Gas Turbine Conference and Exhibition, Anaheim, California — May 31-June 4, 1987

flows typical of turbomachines and to attempt to avoid confusion of terms, we will use the terms "rotor-wake-generated" unsteadiness to describe the unsteadiness generated by the rotor wake velocity deficit, and "unresolved" unsteadiness to refer to the remaining unsteadiness.

Recent experimental investigations of the unsteady flows in high-speed compressors (1) and turbines (2-4) have revealed several phenomena associated with blade-row interactions. Using a laser transit anemometer (LTA) to investigate the unsteady interactions within a compressor stator row, Dunker (1) was able to identify rotor wake segments and the distribution of unresolved unsteadiness throughout the stator row. Similarly, Binder (2-4) used an LTA to investigate unsteady interactions within a turbine rotor. Binder observed an increase in unresolved unsteadiness near the rotor leading edge which he concluded was a result of the rotor chopping the stator secondary vortex.

In the present experimental investigation, a laser fringe anemometer (LFA) was used to measure the unsteady velocity field within a transonic axial-flow fan stator row. Measurements were obtained for two different stator configurations - a stator row consisting of double-circular arc (DCA) blade shapes and a stator row consisting of controlled-diffusion (CD) blade shapes. The measurement and analysis techniques used to resolve the unsteady flow field features are described in Part I of this paper. Mean flow field results are presented as well as the spatial distributions of "rotor-wake-generated" and "unresolved" velocity correlations. The results support many of the conclusions arrived at in earlier investigations and also provide some new insight into the growth and decay of unsteady velocity fluctuations caused by blade-row interactions.

TEST COMPRESSOR AND LASER ANEMOMETER SYSTEM

The research vehicle used in this work is a single stage transonic axial-flow compressor. The design-speed is 16043 rpm and the corrected mass flow rate is 34 kg/s. Since the fan stage was designed for low noise, the rotor and stator are separated by approximately 85 percent rotor chord at midspan. The strength of the rotor wakes and the related blade-row interactions are therefore significantly diminished from what would occur in a more closely coupled stage. The advantage of the wide axial spacing between blade rows is reduction of the potential flow-field interactions between the blade rows. Rotor-wake-generated unsteady effects can thus be studied independently of the potential flow influence in this fan stage.

The rotor is a damperless fan composed of 22 blades of multiple-circular-arc design. The rotor aspect ratio is 1.55 (average span/mid-chord) with an inlet tip diameter of 51.3 cm and inlet hub/tip radius of 0.375. The rotor tip clearance is 0.5 mm. Details of the rotor aerodynamic design are given in Ref. 5.

The double-circular-arc stator blade row was designed to discharge fluid axially and to have a constant axial chord from hub to tip of 5.6 cm. The stator consists of 34 blades with a midspan solidity of 1.68. The stator tip diameter is constant at 48.7 cm and the inlet and exit hub/tip radius ratios are 0.500 and 0.530 respectively.

The controlled-diffusion stator blade row consists of 17 blades with a midspan solidity of 0.85. The CD blade row was designed to provide the same performance as the DCA stator design with the following constraints: (1) use one-half the number of blades as the DCA stator, (2) eliminate boundary layer separation from the blade surface, and (3) use the same flowpath geometry as the DCA stator. The resulting blade has a polynomial blade shape which provides the flow turning rates required throughout the stator passage to achieve the maximum blade loading without boundary layer separation. In addition, a relatively high negative incidence angle is required to avoid a potential flow separation at the stator leading edge which was indicated in the predicted suction surface velocity distribution. The design parameters for both the DCA stator and the CD stator are presented in Table I.

The stator flow field was surveyed on a midspan axisymmetric measurement surface at the measurement locations shown in Fig. 1. At each axial location the data were acquired at 10 circumferential locations evenly distributed between 5 and 95 percent stator gap. The stator gap is measured relative to the pressure surface of the blade. At each survey location, laser anemometer measurements were recorded for 50 different circumferential locations across a rotor rotation of one pitch. Only velocity components which lie in the axial-circumferential plane were measured. Further details of the measurement techniques are given in Part I of this paper.

PRESENTATION AND DISCUSSION OF RESULTS

Data are presented for the following cases at design-speed: (1) DCA stator blade operating at peak efficiency, (2) CD stator blade operating at peak efficiency, and (3) CD stator blade operating at near-stall. These three cases are compared to provide some assessment of the effects of blade loading, incidence angle, and the stator solidity on the unsteady flow field within a stator passage. Both the steady and unsteady descriptions of the stator flow field are presented. Based on the measured results, correlations of the rotor-wake-generated and unresolved unsteady-velocity fluctuations are used to study the unsteady blade-row interactions. Refer to Part I of this paper for a description of the measurement and analysis techniques used to obtain the parameters which describe the steady-state and the unsteady flow-field features presented below.

Steady-State Flow Field Description

Contour plots of the total absolute velocity (V_T) for the DCA stator operating at peak efficiency and for the CD stator operating at peak efficiency and near stall are presented in Fig. 2. All contour plots presented in this paper are generated by translating the data measured in one stator passage by one stator pitch before calling the contour plot program. Consequently, the plotting program has no knowledge of the presence of the center blade shown in Fig. 2 and therefore utilizes standard interpolation techniques to generate contour lines between the lower and upper blade passages which cross the center blade. In all contour plots presented herein, one should therefore study the contours near the lower and upper blade in order to draw conclusions about the flow-field behavior near the pressure and suction surface respectively.

The inlet freestream velocity (V_{FS}) is approximately 235 m/s for the DCA stator blade row and approximately 225 m/s for the CD stator blade row. The axisymmetric mean incidence angles determined from conventional pressure probe surveys performed at a station between the rotor and stator are approximately +1° for the DCA stator operating at peak efficiency and -17 and -12° for the CD stator operating at peak efficiency and near-stall respectively. Observe from Fig. 2 that as the mean incidence angle becomes more negative, the region of high velocity near the leading edge of the stator suction surface becomes larger and

is pushed further downstream. The effect of increased blade loading can be seen by comparing the velocity gradient across the blade passage in the circumferential direction in the DCA stator to that in the CD stator.

Figure 2 also shows the upstream extent of the potential flow-field effect due to the presence of the stator blades. Using the criteria that any circumferential variation in the total absolute velocity which occurs upstream of the blade row is due to the stator potential influence, the potential field of the DCA stator is observed to extend to about 30 percent of stator axial chord upstream of the leading edge. The potential field for the CD stator appears to extend to at least 40 percent of stator axial chord upstream of the stator leading edge. This is probably a result of the large negative incidence angle of the CD blade which causes a greater flow adjustment around the leading edge in comparison to the DCA blade. Also note that since the rotor trailing edge is almost 100 percent of stator axial chord upstream of the stator leading edge, the potential interactions between the stator and rotor are very weak. Although acoustic interactions may still be present, the only significant blade-row interactions are due to rotor-wake-generated and unresolved unsteadiness.

Rotor Wake Chopping

Figure 3 shows a sequence of plots for a rotor rotation of one pitch which depict the rotor wakes as they are chopped and subsequently transported through the DCA stator blade row. The shaded regions identify rotor wake fluid and were determined by normalizing the unresolved unsteadiness at each point in the stator flow field so that the background (i.e., free stream) unresolved unsteadiness is zero and the maximum unresolved unsteadiness (which is expected to occur within the rotor wake) is set equal to one (6). The shaded regions represent areas in which the level of the normalized unresolved unsteadiness is greater than 0.25. Similar contour plots depicting the movement of wakes through adjacent blade rows have been presented by Dunker (1) for a compressor blade row and Binder (2) for a turbine blade row.

From Fig. 3 one can see that after the stator blade chops the rotor wake, the wake segments move at different speeds along the stator blade pressure and suction surfaces. By the time the rotor wake segments reach the stator exit, there is an appreciable mismatch or "drift" between the rotor wake segments which were originally part of the same rotor wake. Using linear small-disturbance theory, Smith (7) has shown that for thin airfoils with relatively little turning this drift distance can be related to the airfoil circulation, Γ, and the average of the inlet and exit velocities, V_A, according to the following equation:

$$\Delta S = \frac{\Gamma V_E}{V_A^2} \tag{7}$$

where

$$\Gamma = \frac{2\pi}{N_S}\left(R_I V_{\theta I} - R_E V_{\theta E}\right) \quad \text{and} \quad V_A = \frac{V_I + V_E}{2}$$

The drift distance, ΔS, is measured along the extension of the stator trailing edge mean camber line. Table 2 shows a comparison between the calculated and measured drift distances along the 50 percent span measurement surface of the DCA stator, expressed as a percentage of stator axial chord. Joslyn et al. (8) used an inviscid analysis to successfully predict the motion of a narrow smoke stream (i.e., an inviscid zero-velocity-deficit "wake") through a downstream rotating blade row by tracing isochronous lines measured relative to the initial upstream generated smoke stream. For a cusped leading edge airfoil, their approach reduces to that of Smith (7).

It is also evident from Fig. 3 that the rotor wakes tend to pile up at the stator exit, and that there is some slight spreading of the rotor wake width. In light of the above observations, it seems apparent that the kinematics of the transport of rotor wakes through the downstream stator blade row is largely controlled by the steady-state potential flow field. In the present stage the rotor wake has already substantially decayed prior to entering the stator blade row. In a more closely coupled rotor and stator row, where rapid rotor-wake mixing occurs within the stator row and potential interactions are present, a simple inviscid analysis may not be adequate to predict the rotor-wake motion through the stator blade row.

A generally accepted theory, first proposed by Meyer (9), is that a wake behaves like a negative jet. Therefore, when a rotor wake is cut by the stator blade row the width of the wake will tend to diminish on the stator suction surface and increase on the stator pressure surface. Several investigators have since shown experimental evidence in support of this theory (10-13). Most notable was an experimental investigation by Kerrebrock and Mikolajczak (10) which indicated that the higher-energy fluid of the rotor wake tends to impinge and collect on the stator pressure surface, resulting in a marked increase in stagnation temperature on the pressure side of the stator wake. However, there is no apparent evidence in Fig. 3 of the rotor wake width either diminishing on the stator suction surface, or increasing on the pressure surface. Most likely, for this loosely coupled stage, this effect of the rotor wake behaving like a negative jet is quite small since the strength of the rotor wake has weakened considerably by the time it enters the stator passage.

Similar wake transport phenomena were observed in the CD stator blade row. However, due to the higher velocity gradient in the circumferential direction across the blade channel the drift distance of the rotor wake segments within the CD stator passage was greater in magnitude than that measured within the DCA stator passage. Also, since the solidity of the CD stator blade row is half that of the DCA stator blade row, the rotor wake segments were more clearly identified throughout the CD stator passage.

Rotor-Wake-Generated Unsteady-Velocity Correlations

Contour plots of the rotor-wake-generated unsteady-velocity correlations (RWVC) along the 50 percent span measurement surface for the DCA and CD stators are illustrated in Fig. 4. The square of the axisymmetric free stream velocity (V_{FS} = 235 m/s for the DCA stator and V_{FS} = 225 m/s for the CD stator) upstream of the stator is used to normalize the rotor-wake-generated unsteady-velocity correlations. For each of the three test cases, it is apparent that the rotor-wake-generated unsteadiness is highest at the rotor trailing edge and decreases downstream of the rotor trailing edge as a result of the rapid decay of the rotor wake. However, as the flow approaches the stator passage the rotor-wake-generated unsteadiness increases in different regions for each case tested. Contour plots of the RWVC for the three test cases will be compared below in an attempt to assess the effects of incidence angle, blade loading, and stator solidity on the RWVC.

Contour plots of the axial, tangential, and cross-components of the RWVC for the DCA stator are illustrated in Figs. 4(a) to (c). In Fig. 4(a), the normalized axial component of the RWVC decreases from about 0.36 percent V_{fS}^2 at -70 percent stator chord to about 0.16 percent V_{fS}^2 at -20 percent of stator chord. From -20 percent stator chord to the stator exit the axial component of the RWVC continues to decrease to less than 0.04 percent V_{fS}^2 except in a region between -20 and 10 percent of stator chord. In this region the axial component of the RWVC increases near mid pitch and reaches a maximum of about 0.25 percent V_{fS}^2 at 5 percent stator chord. Although considerably weaker, similar increases occur for the tangential and cross components of the RWVC, as indicated in Figs. 4(b) and (c), respectively.

Contour plots of the normalized axial component of the RWVC for the CD stator operating at peak efficiency and near-stall are presented in Figs. 4(d) and (e). The contour plot of the RWVC for the CD stator operating at peak efficiency indicates a decrease in the RWVC from 0.59 percent V_{fS}^2 at the rotor trailing edge to about 0.20 percent V_{fS}^2 at the stator leading edge. In general, the RWVC continues to decrease throughout the stator passage. There is a small local increase in RWVC near -10 percent chord. There is also a localized increase in the RWVC near the stator suction surface from about 65 percent stator chord to 90 percent stator chord which can be seen in Fig. 4(d). The contour plot of RWVC for the CD stator operating at near-stall (Fig. 4(e)) also shows a decrease in RWVC upstream of the stator passage, where the RWVC decreases from 0.59 percent V_{fS}^2 at the rotor trailing edge to about 0.35 percent V_{fS}^2 at -20 percent chord. However, in the region between -20 and -10 percent chord at mid pitch the RWVC increases from 0.32 V_{fS}^2 to 0.42 percent V_{fS}^2. One feature which is common to all three cases shown in Fig. 4 is that the RWVC increases locally in the region near the leading edge between -20 and 10 percent chord. Although not presented here, the tangential and cross-components of the RWVC for the CD stator indicate the same trends as indicated by the axial component of RWVC.

The effects of changing the stator solidity on the rotor-wake-generated unsteadiness can be seen by comparing the contour plot of the axial component of the RWVC for the DCA stator (Fig. 4(a)) to that of the CD stator (Fig. 4(d)). Note that the rotor-wake-generated unsteadiness in the passage of the DCA stator is damped out by about 35 percent chord, while in the CD stator the effects of the rotor-wake-generated unsteadiness are still present up to approximately 65 percent stator chord. This difference may be indicating that the stator chopping of the rotor wake promotes mixing since the DCA stator chops the rotor wakes at twice the frequency of the CD stator.

The effects of changing the incidence angle and blade loading on the rotor-wake-generated unsteadiness can be seen by comparing contour plots of the RWVC for the CD stator operating a peak efficiency and near-stall (Figs. 4(d) and (e)). At the peak efficiency operating point, the RWVC displays local growth near the stator suction surface between approximately 65 and 90 percent chord. At the near-stall condition the RWVC grows locally near mid-pitch between -10 and -20 percent chord. Apparently the change in incidence angle or blade loading is responsible for this change in the location of the regions in which the rotor-wake-generated unsteadiness is amplified.

The physics behind these islands of increased rotor-wake-generated unsteadiness is not understood at this time. However, similar blade-row interaction effects have been observed by Matsuuchi and Adachi (12) and Binder (3-4). The interactions are small for the present stage configuration due to the wide axial spacing between rotor and stator blade rows. Future experiments which are planned in a more closely coupled stage may help to explain these phenomena.

Correlations of Unresolved Velocity Fluctuations

Blade-to-blade distributions of the component of the unresolved unsteady-velocity correlations (UVC) which lies in one of the LFA measurement directions are presented in Fig. 5 for various axial survey stations. The data symbols in the figure represent estimates of the UVC, whereas the bars indicate the 95 percent confidence bands on these estimates. Note that the bands are large because they represent the confidence intervals of a variance. Two LFA measurement directions, +20° and -20° to the steady-state absolute flow angle were used, but since the values of the UVC component in each of the measurement directions showed the same trends, the UVC component in the only one of the measurement directions (+20° direction) is presented. Although the absolute flow angle is approximately constant from blade-to-blade at a given axial location, it varies considerably in the axial direction. Caution should, therefore, be exercised when attempting to draw conclusions from apparent axial gradients in the measured unresolved unsteady-velocity correlations. The magnitude of the unresolved unsteady-velocity correlations are normalized with respect to the square of the axisymmetric free-stream absolute velocity upstream of the stator potential field as was done for the rotor-wake-generated unsteady-velocity correlations.

For the DCA stator, as shown in Fig. 5(a), the component of the UVC in the first measurement direction is approximately constant at about 0.34 percent V_{fS}^2 upstream of the blade row. At about -20 percent stator chord and 15 percent stator gap this component of the UVC begins to increase. This point of increased UVC migrates toward the stator suction-surface with increasing streamwise distance and reaches a maximum value of 0.63 percent V_{fS}^2 at -5 percent stator chord. This component of the UVC then remains above 0.5 percent V_{fS}^2 up to about 20 percent stator chord, beyond which its magnitude becomes obscured by the stator suction-surface boundary layer.

Binder (2-4) observed a similar increase in unresolved unsteadiness within the vane wake of a single-stage turbine as it was transported through the downstream rotor row. Binder found that the unresolved unsteadiness within the vane wake increased near the rotor leading edge and attributed the increase to cutting of the vane secondary vortices by the rotor which caused the vortices to breakdown, thus generating higher unresolved unsteadiness levels. Although this seems to be a plausible explanation for the increases in the unresolved unsteadiness found by Binder, it does not seem to suffice for an explanation of the observed increases in both the rotor-wake-generated and unresolved unsteady-velocity fluctuations observed in the present research fan. One would expect a breakdown of the secondary vortex to cause increased mixing and therefore a reduction in the rotor wake velocity deficit, which is contrary to the measured increases in the rotor wake velocity deficit indicated from Fig. 4.

The blade-to-blade distributions of the UVC for the CD stator operating at peak efficiency and near-stall are depicted in Figs. 5(b) and (c), respectively. The distributions of the UVC for the CD stator operating at both peak efficiency and near-stall indicate an increase in the UVC from the stator pressure to suction surface throughout the CD stator passage. At the near-stall operating point, the blade-to blade distributions

at -10 and 0 percent stator chord (see Fig. 5(c)) indicate that the large pitchwise gradient in UVC which occurs between 50 and 70 percent of stator gap occurs in the same location as the rapid changes in the RWVC shown in Fig. 4(e). Comparing the CD stator to the DCA stator, note that the increase in UVC from the pressure to the suction surface which occurs in the CD stator does not occur in the DCA stator. The higher blade loading in the CD stator may contribute to this effect.

Increases in the unresolved unsteady-velocity correlations shown in Fig. 5 may be due to an increase in the unresolved unsteadiness either in the "freestream" region between rotor wakes, in the rotor wakes themselves, or in both regions. To resolve this issue, rotor pitchwise variations of the unresolved unsteadiness at several circumferential survey points across the stator pitch for the peak efficiency operating point are shown in Figs. 6(a) and (b) for the DCA and CD stator, respectively. The plots of Fig. 6a correspond to an axial survey station where the rotor-wake-generated unsteadiness displays a local growth. Figure 6(a) indicates that the unresolved unsteady-velocity fluctuations within the wake remain approximately constant blade-to-blade, while the unresolved unsteady-velocity fluctuations within the free stream increase and decrease from blade to blade. Therefore, changes in the magnitude of the UVC at a given axial station within the DCA blade occur as a result of changes in the free-stream unresolved unsteadiness rather than changes in the unresolved unsteadiness within the wake.

Rotor pitchwise distributions of the UVC within the CD stator at 50 percent stator chord are presented in Fig. 6(b). Note that the unresolved velocity fluctuations within the wakes appear to be suppressed near the pressure surface and amplified near the suction surface. The UVC levels in the freestream regions outside of the rotor wake are relatively constant. Therefore, changes in the pitchwise distribution of the UVC in the CD stator shown in Fig. 5 appear to be due to changes in the unresolved unsteadiness within the wake.

Comparison Between Rotor-Wake-Generated and Unresolved Unsteady-Velocity Correlations

In order to evaluate the relative contributions of the RWVC and the UVC to the unsteady flow field, the axisymmetric axial components of the RWVC and the UVC are presented in Fig. 7 for all three test cases. These axisymmetric components are obtained by arithmetically averaging the measured circumferential distributions of the RWVC and the UVC at each axial measurement station. As discussed in Part I of the paper, the axial component of the UVC cannot be determined using the present laser anemometer system, but can be bounded. The axial component of the UVC is therefore presented in the form of the upper and lower bounds which it could attain. Also note that in most cases in Fig. 7 the uncertainty intervals which represent the 95 percent confidence level for the RWVC are the same size as the symbols used to denote the RWVC.

The results presented in Fig. 7 indicate that the decay of the axisymmetric axial component of the RWVC is similar for all three test cases. The relative magnitude of the RWVC and the UVC are also similar for all three cases. Finally, the unresolved unsteady-velocity correlations are consistently greater than the rotor-wake-generated unsteady-velocity correlations, except upstream of the stator leading edge where the values of the RWVC lie within the bounds of the UVC for all three test cases. This last result indicates that through-flow mixing would appear to be largely controlled by the unresolved unsteadiness and not the rotor-wake-generated unsteadiness, at least for the present research fan. As previously mentioned, however, unresolved unsteadiness as defined herein includes any unsteadiness not correlated with the fundamental rotor rotational frequency. In the case of the present research fan, part of the unresolved unsteadiness is due to vortex shedding from the rotor trailing edge (14). This vortex shedding increases the magnitude of the UVC relative to that which would exist in the absence of the shedding. In addition, since the spacing between the rotor and stator in the present stage is wide in comparison to most stages, the rotor wake has significantly decayed before it enters the stator passage. In a more closely coupled stage the effects of the rotor-wake-generated unsteadiness could be substantially larger.

SUMMARY AND CONCLUDING REMARKS

Detailed measurements of the flow field in a DCA stator operating at peak efficiency and in a CD stator operating at peak efficiency and near-stall were compared to assess the effects of blade loading, incidence angle, and the stator solidity on the unsteady flow field within the stator passage. The measurements were acquired along the 50 percent span surface of revolution of each stator with a laser anemometer data acquisition system. The measured velocities were used to determine the magnitudes and distributions of the rotor-wake-generated and the unresolved unsteadiness. Based on the measured data, the following observations were made:

1. The kinematics of the transport of the rotor wakes through the downstream stator row is largely controlled by the steady-state potential flow field.
2. Simple linear disturbance theory is adequate for predicting the drift distance between wake segments convecting along the stator pressure and suction surfaces.
3. Spreading of the rotor wake segments within the stator row appears to be minimal.
4. The rotor-wake-generated unsteadiness persists further downstream within the CD stator passage than within the DCA stator passage, indicating that the chopping of the rotor wake by the stator blade promotes mixing.
5. Contour plots of the RWVC for both the CD and the DCA stator indicate that the wake-generated unsteadiness may be amplified at isolated regions throughout the stator passage. The location of these regions of increased wake-generated unsteadiness is affected by changes in the stator incidence angle.
6. Unresolved unsteadiness within the wakes and the ensemble mean velocity deficit of the wake appears to be suppressed near the pressure surface and magnified near the suction surface of the CD stator.
7. Blade-to-blade increases in the UVC of the DCA stator were due primarily to increases in the free-stream unresolved unsteadiness. However, for the CD stator the increases in the UVC were largely due to increases in the wake unresolved unsteadiness.
8. The unresolved unsteady-velocity correlations are significantly greater than the rotor-wake-generated unsteady-velocity correlations, which indicates that through-flow mixing is largely controlled by the unresolved unsteadiness and not the rotor-wake-generated unsteadiness for the present research fan.

At present, a satisfactory explanation for the presence of the increased rotor-wake-generated and unresolved unsteadiness near the stator leading edge has not been found. It is also unclear what effect, if any, this region of increased unsteadiness has on the stator performance. In a more closely coupled

stage where the blade row interactions are expected to be much greater, this region of increased unsteadiness could impact the performance of the stator by either energizing or separating the stator suction surface boundary layer. In order to further understand the blade-row interactions present in turbomachines, future testing on a more closely coupled stage is being planned. Also, an improved data acquisition system including a two-component laser anemometer system is currently being developed. This improved data acquisition system will enable measurement of the axial and tangential components of the Reynolds normal stresses and the Reynolds shear stresses which cannot be obtained from the measurements in the present investigation.

REFERENCES

1. Dunker, R.J., "Flow Measurements in the Stator Row of a Single-Stage Transonic Axial-Flow Compressor with Controlled Diffusion Stator Blades," Viscous Effects in Turbomachines, AGARD-CP-351, AGARD, France, 1983, pp. 23-1 to 23-13.
2. Binder, A., Forster, W., Kruse, H., and Rogge, H., "An Experimental Investigation into the Effect of Wakes on the Unsteady Turbine Rotor Flow," Journal of Engineering for Gas Turbines and Power, Vol. 107, No. 2, Apr. 1985, pp. 458-466.
3. Binder, A., "Turbulence Production due to Secondary Vortex Cutting in a Turbine Rotor," Journal of Engineering for Gas Turbines and Power, Vol. 107, No. 4, Oct. 1985, pp. 1039-1046.
4. Binder, A., Forster, W., Mach, K., and Rogge, H., "Unsteady Flow Interaction Caused by Stator Secondary Vortices in a Turbine Rotor," ASME Paper 86-GT-302, June 1986.
5. Urasek, D.C., Gorrell, W.T., and Cunnan, W.S., "Performance of Two-Stage Fan Having Low-Aspect-Ratio, First-Stage Rotor Blading," NASA TP-1493, 1979.
6. Hathaway, M.D., "Unsteady Flows in a Single-Stage Transonic Axial-Flow Fan Stator Row." PhD Dissertation, Iowa State University, 1986.
7. Smith, L.H., Jr., "Secondary Flow in Axial-Flow Turbomachinery," Transactions of the ASME, Vol. 77, No. 7, Oct. 1985, pp. 1065-1076.
8. Joslyn, H.D., Caspar, J.R., and Dring, R.P., "Inviscid Modeling of Turbomachinery Wake Transport," Journal of Propulsion and Power, Vol. 2, No. 2, Mar.-Apr. 1986, pp. 175-180.
9. Meyer, R.X., "The Effect of Wakes on the Transient Pressure and Velocity Distributions in Turbomachines," Transactions of the ASME, Vol. 80, Oct. 1958, pp. 1544-1552.
10. Kerrebrock, J.L., and Mikolajczak, A.A., "Intra-Stator Transport of Rotor Wakes and Its Effect on Compressor Performance," Journal of Engineering for Power, Vol. 92, No. 4, Oct. 1970, pp. 359-368.
11. Ng, W.F., and Epstein, A.H., "A Quasi-Three-Dimensional Model for Intra-Stator Transport of Rotor Wakes," Three-Dimensional Flow Phenomena in Fluid Machinery, A. Hamed, H.J. Herring and L.A, Povinelli, eds., ASME, New York, 1985, pp. 103-111.
12. Matsuuchi, K., and Adachi, T., "Measurement of the Three-Dimensional Unsteady Flow Inside a Rotor Blade Passage of an Axial-Flow Fan," 1983 Tokyo International Gas Turbine Congress, Vol. 2, Gas Turbine Society of Japan, Tokyo, 1984, pp. 523-530.
13. Hodson, H.P., "Measurement of the Wake-Generated Unsteadiness in the Rotor Passages of Axial-Flow Turbines," ASME Paper 84-GT-189, June 1984.
14. Hathaway, M.D., Gertz, J.B., Epstein, A.H., and Stazisar, A.J. "Rotor Wake Characteristics of a Transonic Axial Flow Fan," AIAA Journal, Vol. 24, No. 11, Nov. 1986, pp. 1802-1810.

TABLE I. - STATOR DESIGN PARAMETERS

PARAMETER	DCA STATOR	CD STATOR
Number of blades	34	17
Aspect ratio	2.05	2.02
Solidity at midspan	1.682	0.85
Mean design incidence angle	2.7 deg	-14.0 deg
Turning rate	constant	variable
Midspan aerodynamic chord	5.773 cm	5.832 cm
Midspan axial chord	5.593 cm	5.532 cm
Midspan rotor-stator spacing	85 percent rotor chord	85 percent rotor chord
Constant tip radius	24.384 cm	24.384 cm
Inlet hub/tip radius ratio	0.5	0.5
Outlet hub/tip radius ratio	0.53	0.53

TABLE II. - COMPARISON BETWEEN CALCULATED AND MEASURED ROTOR WAKE SEGMENT NON-DIMENSIONAL DRIFT DISTANCE FOR THE 50 PERCENT SPAN MEASUREMENT SURFACE OF THE DCA STATOR.

PARAMETER	SYMBOL	PERCENT SPAN MEASUREMENT SURFACE VALUE
Stator axial chord	C	5.6 cm
Stator inlet		
Radius	R_I	18.5 cm
Tangential velocity	$V_{\theta I}$	150 m/s
Total velocity	V_I	235 m/s
Stator exit		
Radius	R_E	18.68 cm
Tangential velocity	$V_{\theta E}$	0 m/s
Total velocity	V_E	185 m/s
Drift distance		
Measured	ΔS	34.6 percent C
Calculated		38.4 percent C

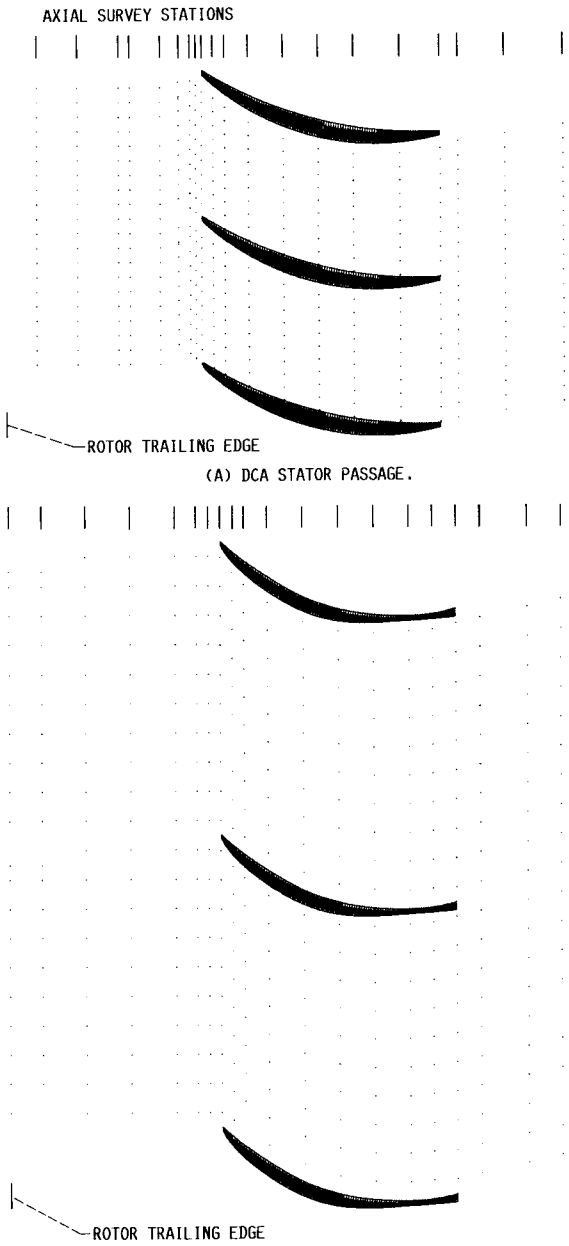

FIGURE 1.- BLADE-TO-BLADE VIEW OF THE MIDSPAN SURFACE SHOWING THE LASER ANEMOMETER MEASUREMENT SURVEY POINTS.

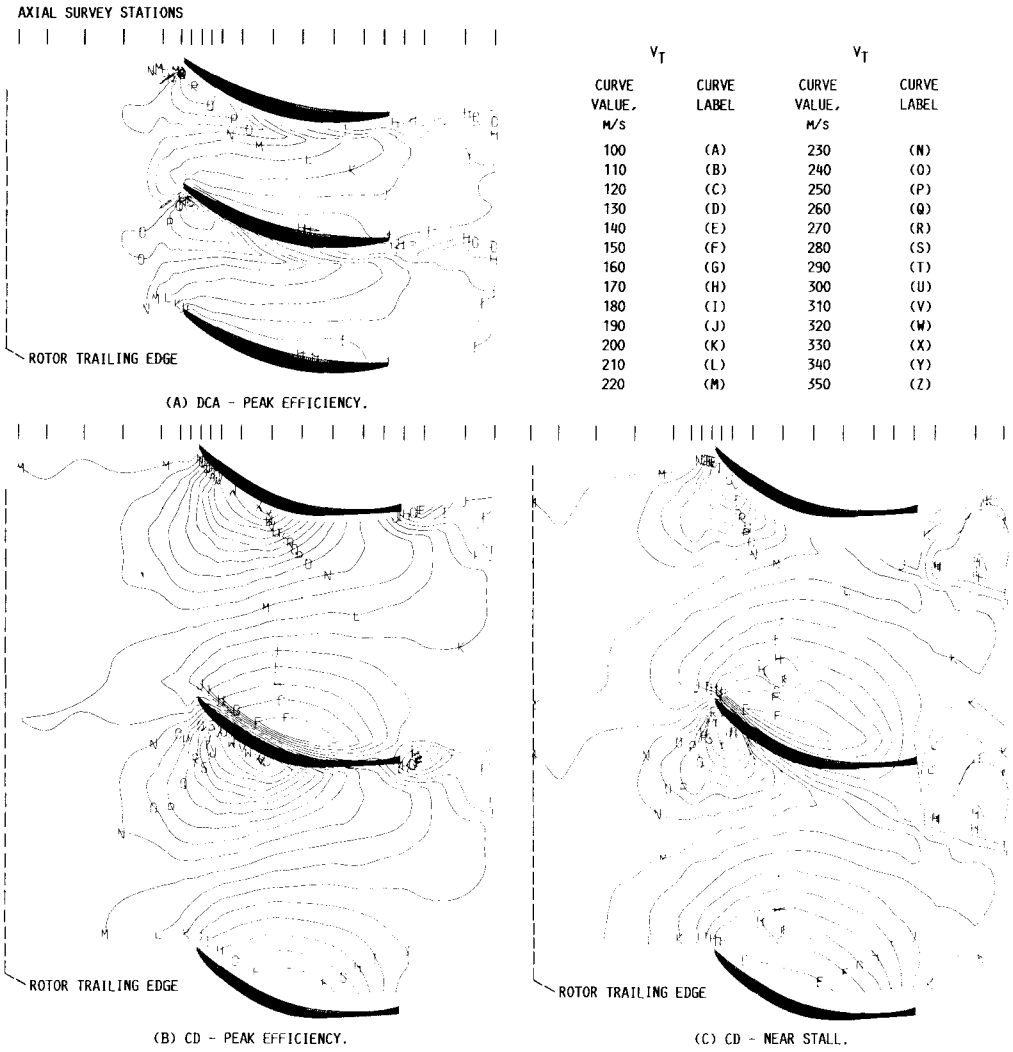

V_T CURVE VALUE, M/S	CURVE LABEL	V_T CURVE VALUE, M/S	CURVE LABEL
100	(A)	230	(N)
110	(B)	240	(O)
120	(C)	250	(P)
130	(D)	260	(Q)
140	(E)	270	(R)
150	(F)	280	(S)
160	(G)	290	(T)
170	(H)	300	(U)
180	(I)	310	(V)
190	(J)	320	(W)
200	(K)	330	(X)
210	(L)	340	(Y)
220	(M)	350	(Z)

(A) DCA - PEAK EFFICIENCY.

(B) CD - PEAK EFFICIENCY.

(C) CD - NEAR STALL.

FIGURE 2.- CONTOUR MAPS OF THE STEADY-STATE ABSOLUTE VELOCITY FIELD ALONG THE 50 PERCENT SPAN MEASUREMENT SURFACES.

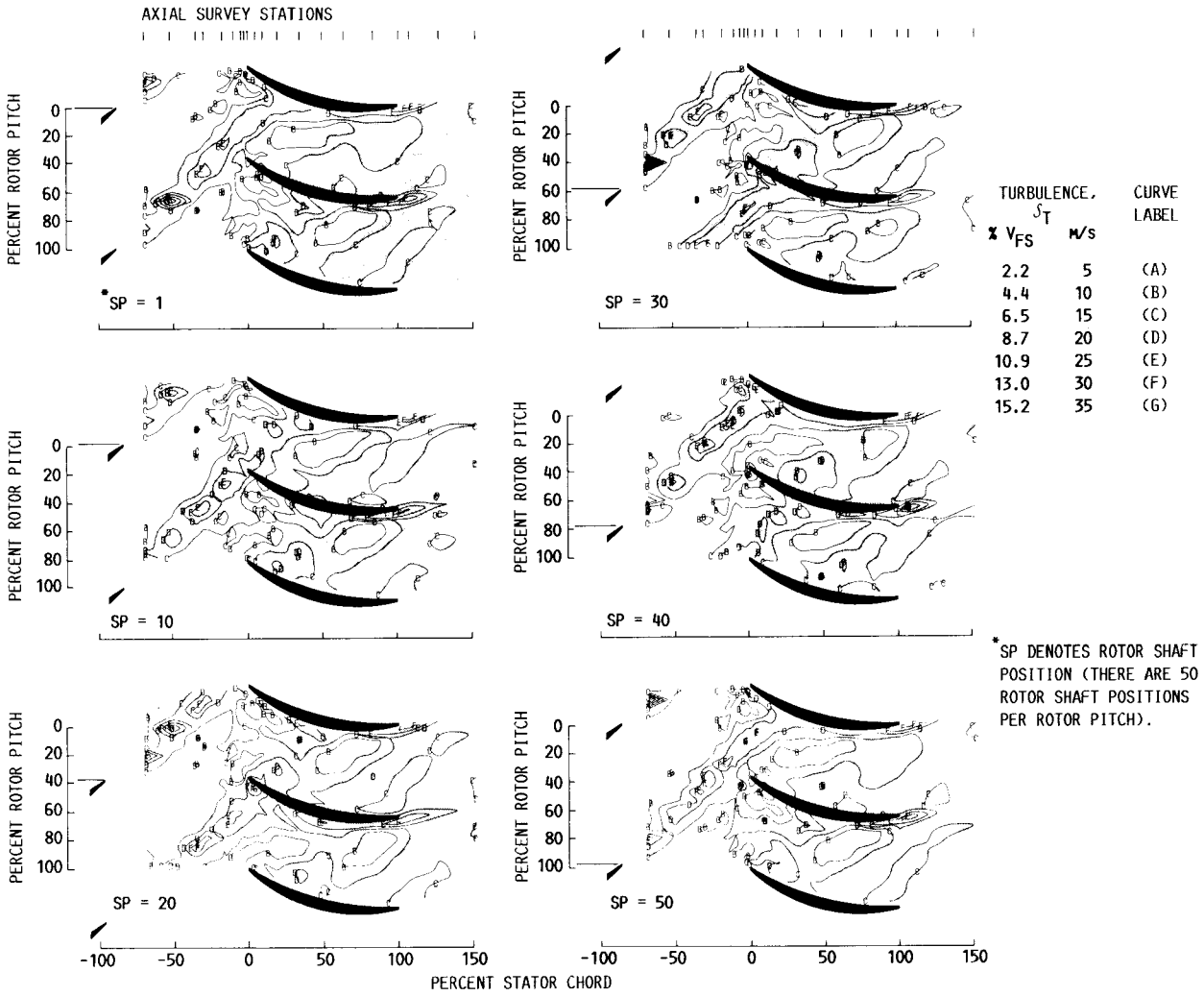

FIGURE 3. - ENSEMBLE-AVERAGE DESCRIPTION OF THE KINEMATICS OF ROTOR WAKE TRANSPORT THROUGH THE DCA STATOR ROW FOR THE 50 PERCENT SPAN MEASUREMENT SURFACE.

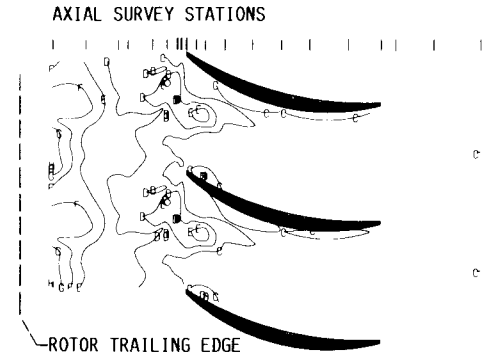

(A) DCA STATOR - PEAK EFFICIENCY $\overline{\tilde{v}_z \tilde{v}_z} / v_{FS}^2 \times 100$.

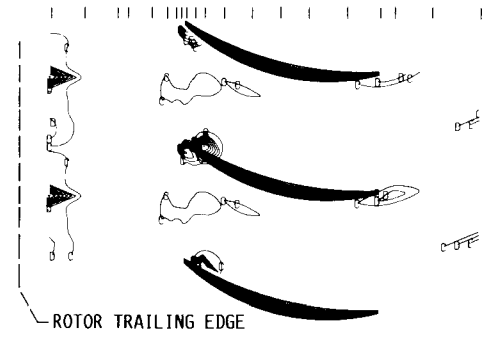

(B) DCA STATOR - PEAK EFFICIENCY $\overline{\tilde{v}_\theta \tilde{v}_\theta} / v_{FS}^2 \times 100$

$\overline{\tilde{v}_i \tilde{v}_i} / v_{FS}^2 \times 100$

CURVE VALUE,	CURVE LABEL
-0.07	(A)
0.0	(B)
0.07	(C)
0.14	(D)
0.22	(E)
0.29	(F)
0.36	(G)
0.43	(H)
0.50	(I)

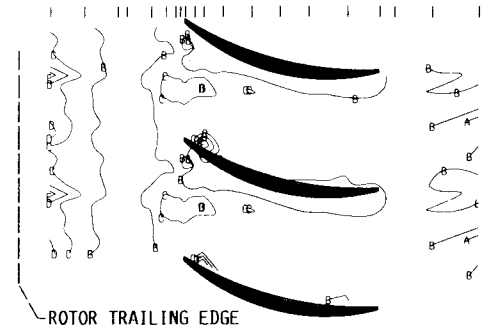

(C) DCA STATOR - PEAK EFFICIENCY $\overline{\tilde{v}_z \tilde{v}_\theta} / v_{FS}^2 \times 100$

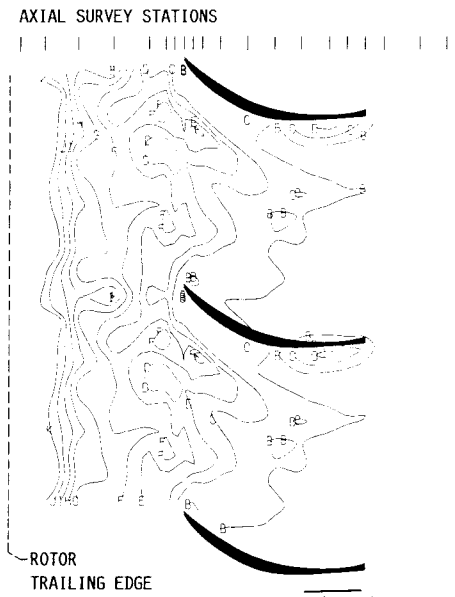

(D) CD STATOR - PEAK EFFICIENCY $\overline{\tilde{v}_z \tilde{v}_z} / v_{FS}^2 \times 100$

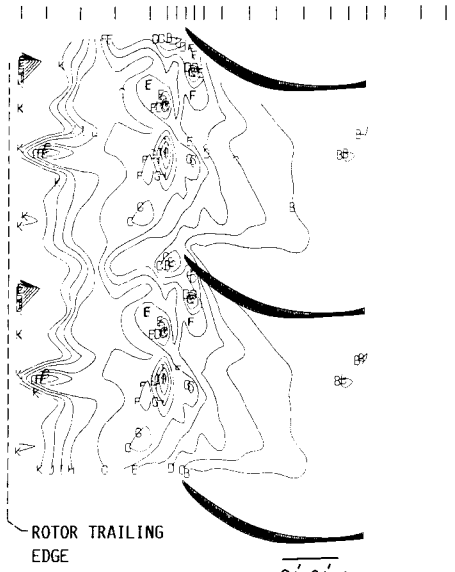

(E) CD STATOR - NEAR STALL $\overline{\tilde{v}_z \tilde{v}_z} / v_{FS}^2 \times 100$

$\overline{\tilde{v}_z \tilde{v}_z} / v_{FS}^2 \times 100$

CURVE VALUE	CURVE LABEL
0	A
0.06	B
0.12	C
0.18	D
0.24	E
0.30	F
0.36	G
0.41	H
0.47	I
0.53	J
0.59	K

FIGURE 4. - CONTOUR MAPS OF THE ROTOR-WAKE-GENERATED UNSTEADY-VELOCITY CORRELATIONS ALONG THE 50 PERCENT SPAN MEASUREMENT SURFACE.

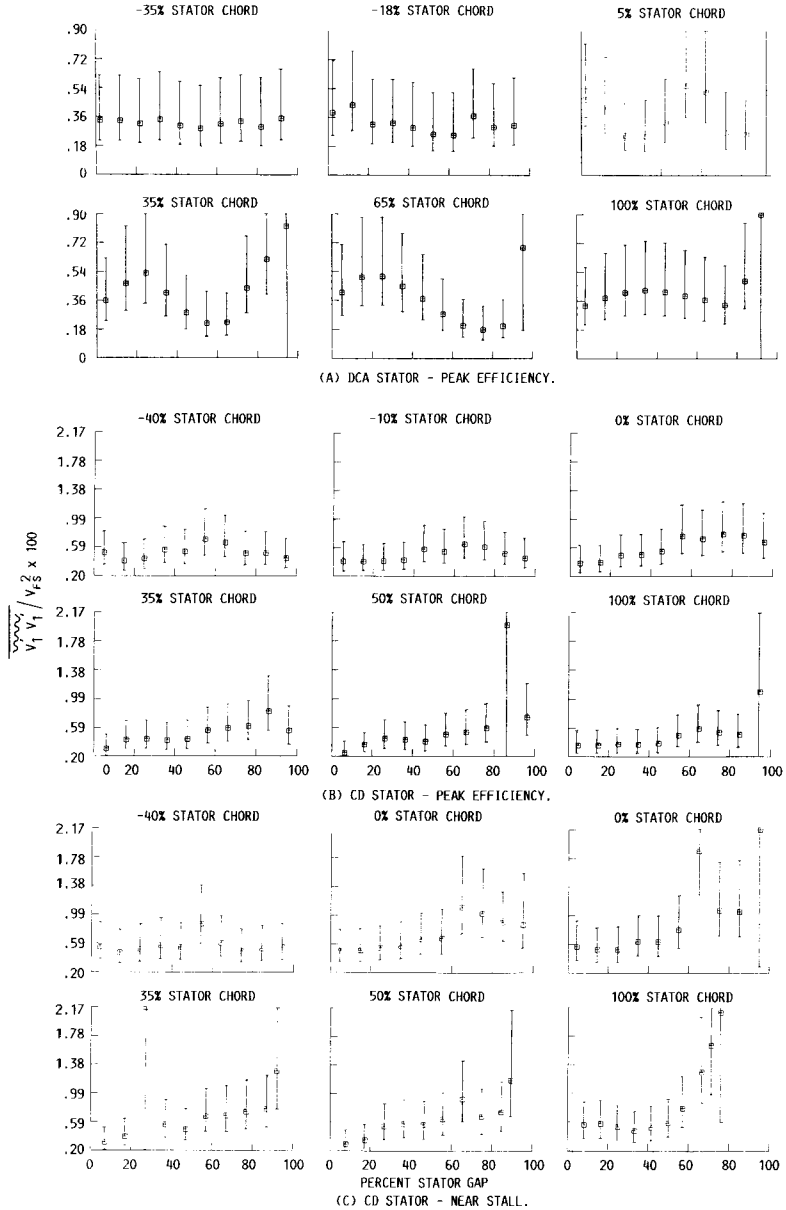

FIGURE 5.- STATOR BLADE-TO-BLADE DISTRIBUTIONS OF THE UNRESOLVED UNSTEADY-VELOCITY CORRELATIONS ALONG THE 50 PERCENT SPAN MEASUREMENT SURFACE.

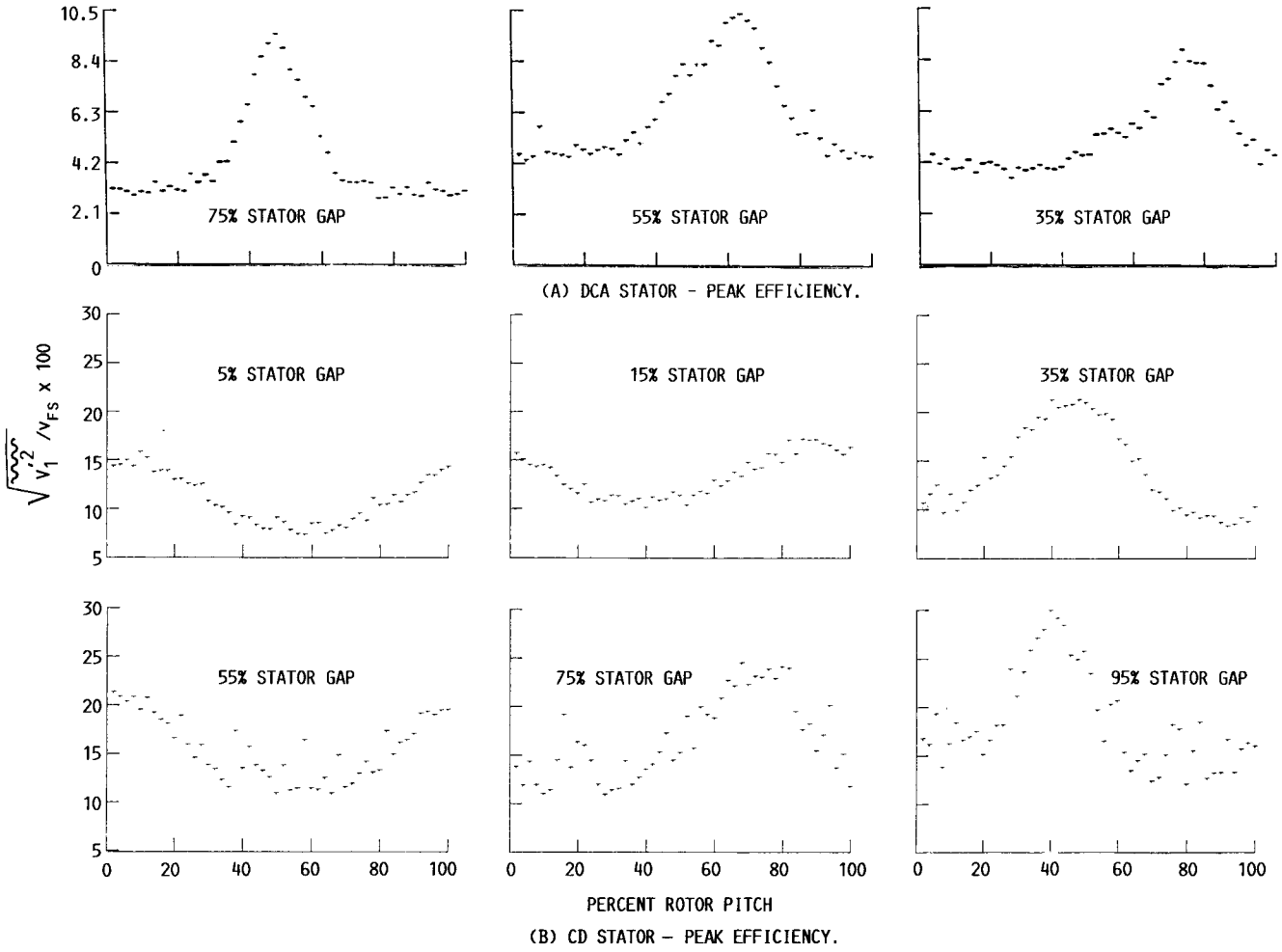

(A) DCA STATOR - PEAK EFFICIENCY.

(B) CD STATOR – PEAK EFFICIENCY.

FIGURE 6.- ROTOR PITCHWISE VARIATION IN THE UNRESOLVED UNSTEADINESS AT SEVERAL BLADE-TO-BLADE SURVEY POINTS.

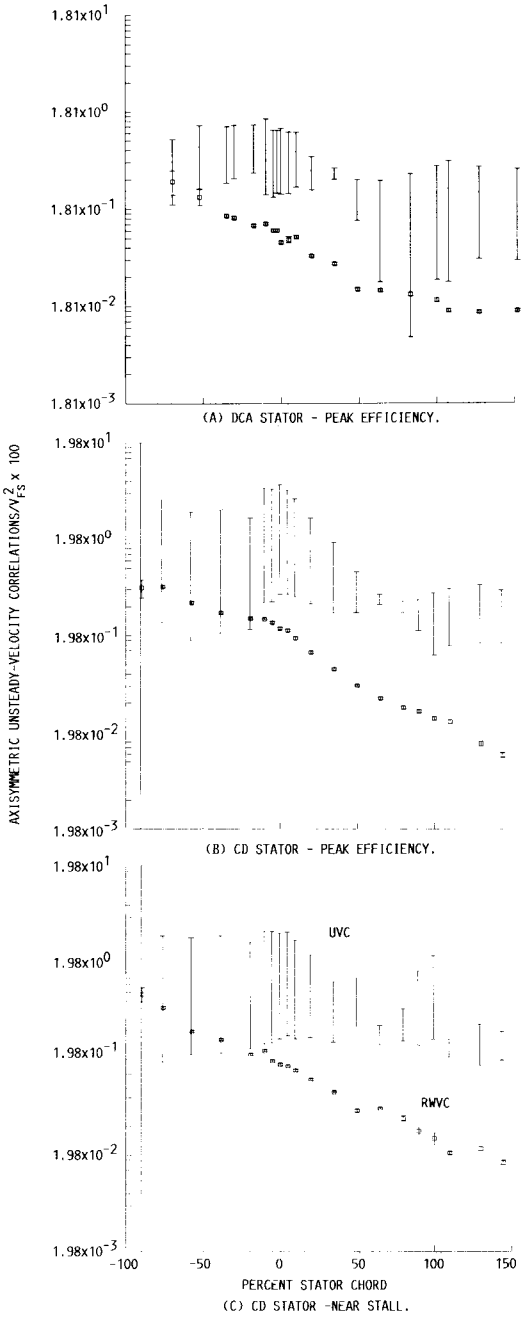

FIGURE 7.- COMPARISON BETWEEN THE AXISYMMETRIC VALUES OF THE ROTOR-WAKE-GENERATED AND UNRESOLVED UNSTEADY-VELOCITY CORRELATIONS ALONG THE 50 PERCENT SPAN MEASUREMENT SURFACE.